Structural and optical study of ZnO-TiO₂ nanocomposites

K. P. Sridevi[a], L. Guru Prasad[b], B. Sangeetha[c], S. Sivakumar[d,*]
aDepartment of Physics, Sri Kailash Women's College, Thalaivasal, India
bDepartment of Physics, M.Kumarasamy College of Engineering, Karur, India
cDepartment of Electrical & Electronics, AVS Engineering College, Salem
dDepartment of Physics, Government Arts College (Autonomous), Salem, India.

Nanocomposites of ZnO-TiO₂ were synthesized by using zinc chloride, titanium tetrachloride, ethanol and benzyl alcohol and diethyl ether by using Sol-Gel technique. Crystalline nature of the prepared material was analyzed using XRD study. Band gap of the material found at 3.05eV. In the PL spectra, the peak giving emission is found at 430nm and at 615nm. To confirm the ferromagnetic ordering, the VSM study was done. Morphology study was carried out with SEM images.

1. Introduction

In recent years due to the notable electronic and chemical properties, metal oxide nanoparticles captivate more recognition. Considering the chemical solidity and well-organized photocatalytic properties among the metal oxide semiconductors, Zinc Oxide (ZnO) as well as TiO₂ have been investigated extensively. ZnO is used in various fields in different areas like optical, piezoelectric, magnetic and gas sensing properties [1]. Titanium oxide (TiO₂) is extensively utilized in paints, electronic gadgets, gas sensors as well as solar cells [2-5]. It has semiconducting property with super photocatalytic character and broadly utilized in environmental pollutant elimination, antibacterial dopes, auto clean buildings [6-8]. It was found that for most of the photocatalytic decomposition processes, the efficiency is comparatively low and further it was found that the photocatalytic reactions on TiO₂ can be induced only by the UV light. Due to this limitation, the application of TiO₂ as a photocatalyst cannot be studied with the visible light. The photocatalytic nature of TiO₂/ZnO has been studied to increase the photo degradation efficiency of TiO₂ as a photocatalyst. Currently many papers have been reported for enhancing the photocatalytic activity of TiO₂.

In many of the photo catalytic activity, the photocatalysts are altered by doping with ion or by joining TiO₂ with other oxides, for example to ZnO [9-12]. More number of researchers have analyzed the coupled photocatalyst semiconductor ZnO/TiO₂ to increase the effectiveness of photo degradation and the effects for enhancing the efficiency have been described [13-14]. Preparation mechanism of ZnO-TiO₂ nanocomposites and its characterization have been given in this manuscript.

2. Experimental Details

2.1. Materials and Methods

The various chemicals like zinc chloride, titanium tetrachloride, ethanol, benzyl alcohol and diethyl ether were purchased in analytical grade and the entire chemicals were utilized as such without any additional purification.

---

* Corresponding author: sivaphotonics@gmail.com

Utilizing the sol-gel method the ZnO-TiO$_2$ nanoparticles were synthesized. For the synthesis, 1M ZnCl$_2$ was dissolved in 10ml of ethanol to get a solution. By stirring the obtained solution continuously, 50ml of benzyl alcohol was added at room temperature. The added benzyl alcohol serves as a solvent and as well as a reagent and interacts with the different metal chlorides to synthesize series of metal oxides and compound oxides. To this mixture, 1M TiCl$_4$ was added gradually. The Orange liquid so obtained was stirred constantly at 60°C for 8 hours and was kept for aging at room temperature. This was centrifuged with 4500 rpm for 15 minutes which yields white thick precipitates and the precipitates were removed by decantation. The separated precipitate was washed with absolute ethanol for two times and with diethyl ether three times. By the centrifugation process the solvent was segregated at the end of every washing and material only is collected. This material was dried overnight and crushed to form a fine powder. When this powder was calcinated at 200°C it yields ZnO nanocomposites. Fig.1 summarizes the various steps involved in the synthesis of ZnO-TiO$_2$ nano composites.
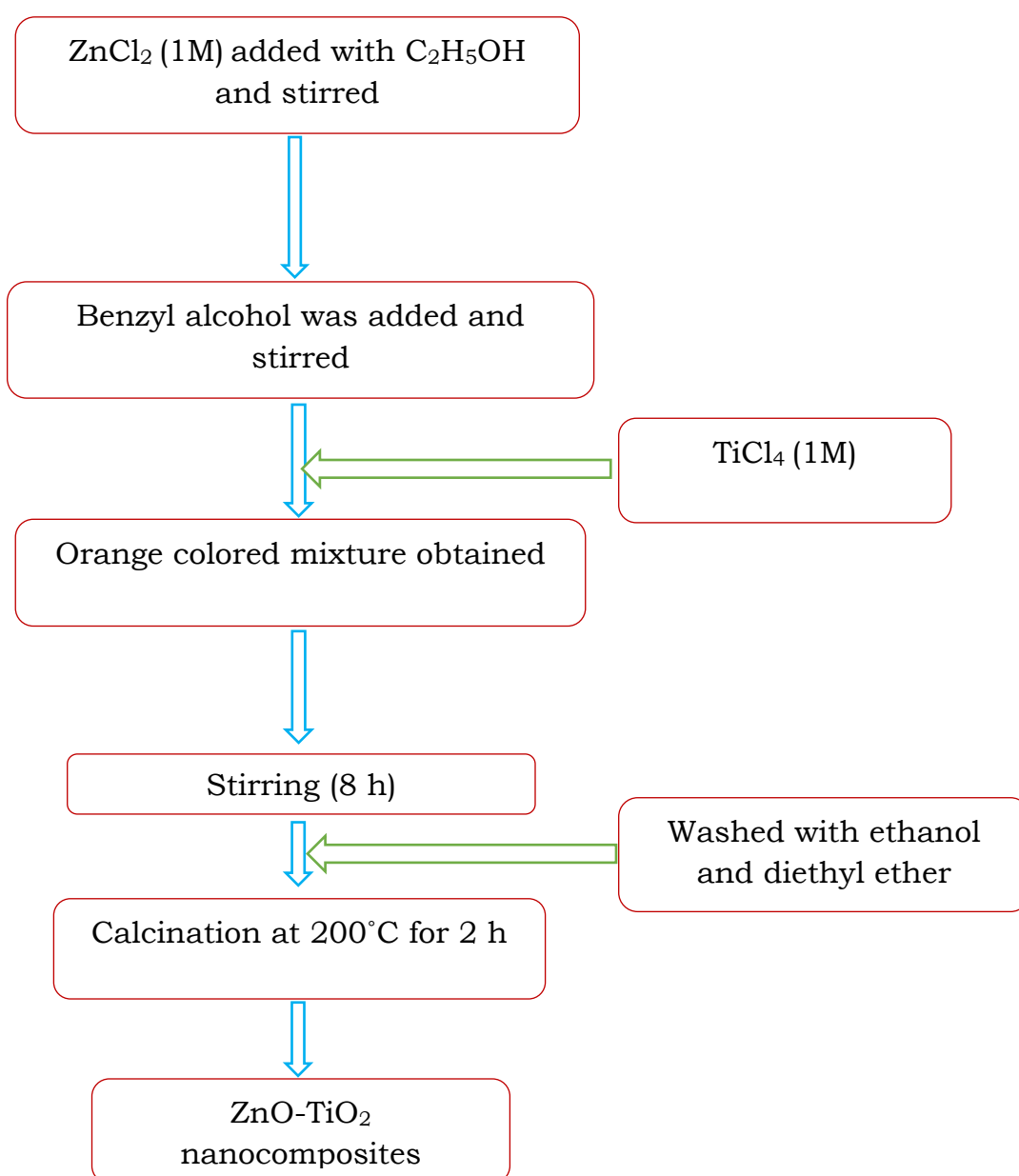

Fig. 1. Steps involved in the synthesis of ZnO-TiO$_2$ nanocomposites.

3. Characterization method

Structure of the ZnO-TiO₂ nanocomposites have been investigated by analyzing the XRD patterns recorded using Riagu Mini Flexell desktop Diffractometer (Using CuKα radiation at a wavelength of 1.5406 Å). Making use of UV–VIS spectrophotometer (JASCO-V-670) in the wavelength range of 300-1000 nm, the optical properties have been studied. Adopting photoluminescence spectrometer (HORIBA Jobin Yvon) with 325 nm He-Cd laser photoluminescence measurements have been taken. By using the Lake Shore 7404 vibrating sample magnetometer instrument, the magnetic properties of the nanocomposites were studied. The structures have been observed with the aid of JEOL 7001F Field emission scanned electron microscopy (FESEM) furnished with EDS to observe the elemental composition. Utilizing JEOL JEM 2100 Transmission electron microscope TEM images have been noticed.

3.1. Structural analysis

The Fig.2 exhibits the XRD patterns of ZnO-TiO₂ nanocomposites. Crystalline nature was confirmed by the XRD patterns. The obtained XRD pattern of the ZnO-TiO₂ nanocomposites have been verified with the standard data of ZnO (JCPDS Card No. 80-0075) and along with TiO₂ (JCPDS Card No. 89-4921). The existence of peaks due to diffraction shown at planes 100, 002, 101, 102, 110, 103, 200,112, 201 and 202 corresponds to ZnO Hexagonal Wurtzite phase. In addition, it was found that the peaks at 101, 004, 200, 105 and 211 planes are in correspondence with TiO₂ diffraction peaks due to the total incorporation of Ti into the structure of ZnO [15-16]. From the observed peaks the corresponding planes were indexed in Fig. 2. Furthermore, the intensity of the ZnO peaks decreased due to TiO₂ has been fused to the ZnO matrix.
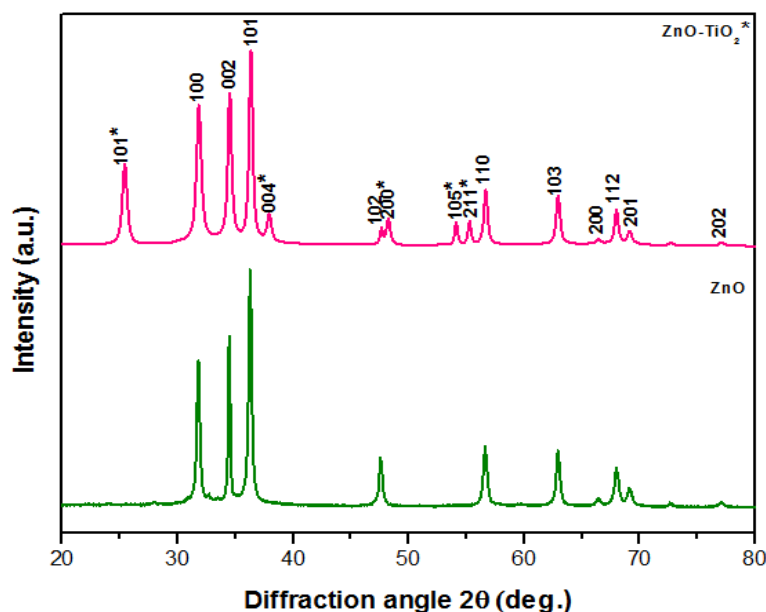

Fig. 2. The XRD patterns of ZnO-TiO₂ nanocomposites.

Utilizing the Scherer's formula, the size of the crystallite has been calculated from the XRD data and it is shown in the Table 1.

$$D = \frac{K\lambda}{\beta \, Cos \, \theta} \, (nm)$$

The dislocation density (δ) is estimated using the equations,

$$\delta \;=\; \frac{15\,\beta\,cos\theta}{4\alpha D}\;\; lines\,/\,m^2$$

Micro strain (ε) is calculated using,

$$\varepsilon = \frac{\beta}{4\tan\theta}$$

Due to the presence of stacking faults, a shift in the position of the peaks is observed in the different reflection planes concerning to the ideal position of peaks of a fault free sample. The correlation among the stacking fault probability (α) with the shift in the peaks in terms of (β) is given by the expression

$$\alpha \;=\; \left[\frac{2\pi^2}{45(3\tan\theta)^{\frac{1}{2}}}\right]\beta\;(\text{Å})$$

where, α - is the stacking fault, β - is the full width at half maximum.

From the Table 1 it has been found that, when TiO_2 was incorporated into the ZnO matrix the crystallite size gets reduced as compared with pure ZnO nanoparticles. The dislocation density, stacking fault and elastic strains are found to be increased. Hence it is confirmed from the XRD studies that the ZnO–TiO_2 nanocomposites have good crystalline nature and it is confirmed that sol-gel is considered as a valuable technique to synthesize poly crystalline ZnO-TiO_2 nanocomposites with fine quality.

Table 1. Structural parameters of ZnO-TiO$_2$ nanocomposites.

Planes	Crystallite Size D (nm)	Dislocation Density (δ) (10^{15} lines / m^2)	Stacking faults probability (Å)	Elastic strains Ɛ
100	18.24	5.0254	0.0039	0.0072
002	22.51	3.2985	0.0031	0.0054
101	24.22	2.8512	0.0028	0.0048
101*	17.06	5.7419	0.0046	0.0097
004*	21.32	3.6777	0.0031	0.0052
200*	23.58	3.0080	0.0025	0.0038

3.2. Optical properties

The displacement of the absorption band into the visible region was revealed by the optical absorption spectra of ZnO-TiO_2 nanocomposites as shown in the Fig.3. During synthesis, the sediment formed decreases the absorbance and the differences in the absorption is explained by considering the formation of agglomerates in the suspension. This behavior is mostly noticed in the ZnO-TiO_2 samples. The maximum absorption of wave length was found near 380 nm and this was assigned to the electronic transitions taking place between the states located in the energy gap. The states present in the energy gap were formed due to the defects present in the structure of the synthesized sample, which is associated with the band gap value of the ZnO-TiO_2 nanocomposite powder. When the volume ratio of TiO_2 into ZnO is increased a red shift is noticed in the absorption edge. The particle size, morphology and increase in volume ratio of TiO_2 are related to the red shift. Due to red shift, the Fermi level of ZnO- TiO_2 gets altered and as a result the value of band gap energy gets decreased. The band observed at 270 nm is due to the electronic transitions between the states present in the deepest level of the valence band [18].

With the help of the Tauc plot analysis the band gap value of the sample has been calculated. The basic absorption corresponding to the excitation of the electron from the valence

band to the conduction band is responsible for the calculation of optical band gap values. Effective relation between the energy of the incident photon (hv) and the absorption coefficient (α) is given by the equation

$$(\alpha h v) = A(h v - E_g)^n$$

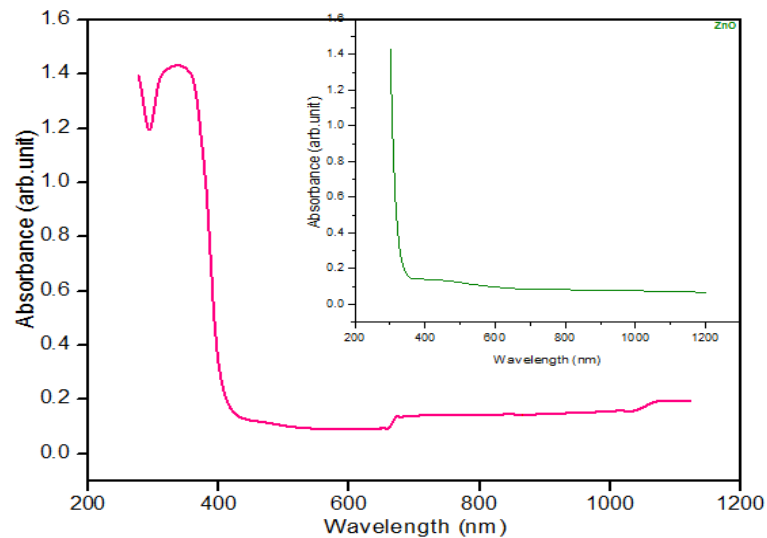Here, Eg is the band gap of the material and the exponent depends on the mode of transition and A is a constant.

Fig. 3. Optical absorbance spectra of ZnO-TiO₂ nanocomposites.

Fig.3 displays a Tauc graph plotted by among $(\alpha h v)^2$ and energy. The linear portions of the graphs were extended to touch the energy axis, from which the energy band gap have been determined as 3.05 eV.
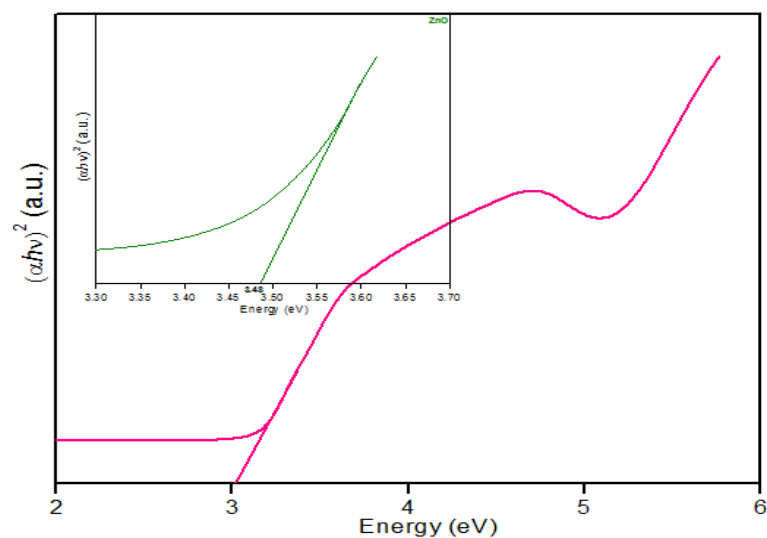

Fig. 4. Optical bandgap of ZnO-TiO₂ nanocomposites.

The inset picture shows the energy bandgap of pure ZnO. It was found that, when the conduction and valance bands expand the band gap value was decreased in ZnO –TiO₂ and this

cause is assigned to the variation in volume ratio of TiO_2 in ZnO which lead the way to modify the band gap from 3.48eV (pure ZnO) to 3.05eV and was similar to the interaction between ZnO and TiO_2. This shift shows the electronic structure (band-band transitions or HOMO-LUMO transitions) have been modified by doping material [19-20].

3.3. Photoluminescence spectroscopy

Photoluminescence spectra of ZnO-TiO_2 nanocomposites was shown in the Fig. 5. In the PL spectra two well described regions has been observed. In the UV region, one peak having high intensity is observed at 430 nm and in the visible region a peak having low intensity is observed at 615nm. The peak at 430nm is related to the NBE emission which occurs due to the exciton transitions. However, it has been observed that the peak in the UV region shift towards larger wavelength (red shift) when TiO_2 was included into the structure. Due to the inclusion of TiO_2 the electronic structure and the band gap value was changed. The red shift is observed due to the creation of impurity states below the conduction band when TiO_2 was doped. Upon doping, defects are produced due to the change in size of the dopant and the host material, and as a result the luminescence of the peak gets enhanced.. In the PL spectra the peaks giving emission at 430 nm is due to the deexcitation of Ti^{3+} 3d states of ZnO-TiO_2 lattice from the lower vibronic level to the deep trap levels. It has been concluded that O_i, Zn_i, V_o and V_{zn} are the defects present in the samples of ZnO-TiO_2 [21-22].
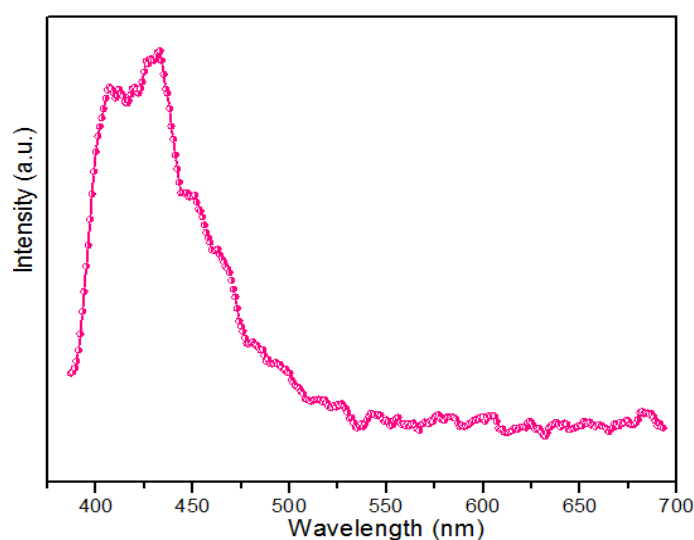

Fig. 5. Photoluminescence (PL) spectra of ZnO-TiO_2 nanocomposites.

3.4. Vibrating Sample Magnetometry (VSM) measurements

By plotting a graph between magnetic moment (M) and the applied magnetic field (H), the magnetic behavior of ZnO-TiO_2 nanocomposites was studied. The existence of the hysteresis loop confirms ferromagnetic ordering in the specimen. It has been observed that the size of the particles formed have dimension of ~17-21nm which was lesser than the critical size (100nm) of the nanoparticles. Each nanoparticle is considered as a domain in which the spins of each domain are in the same direction and the particle is said to be uniformly magnetized. Here it is found that, as there are no domain walls to move, instead of domain wall movement the magnetization is reversed by spin rotation and hence forth the coercivity of the nanoparticles is large. But the observed coercivity is comparatively small, which suggests the spherical nature of the nanoparticles and it is in agreement with the SEM results which suggested the spherical nature of ZnO – TiO_2 nanoparticles. At low coercivity the ferromagnetic nanoparticles will behave like paramagnetic with large spin and when the coercivity turns to zero, the nanoparticles become super magnetic [23].
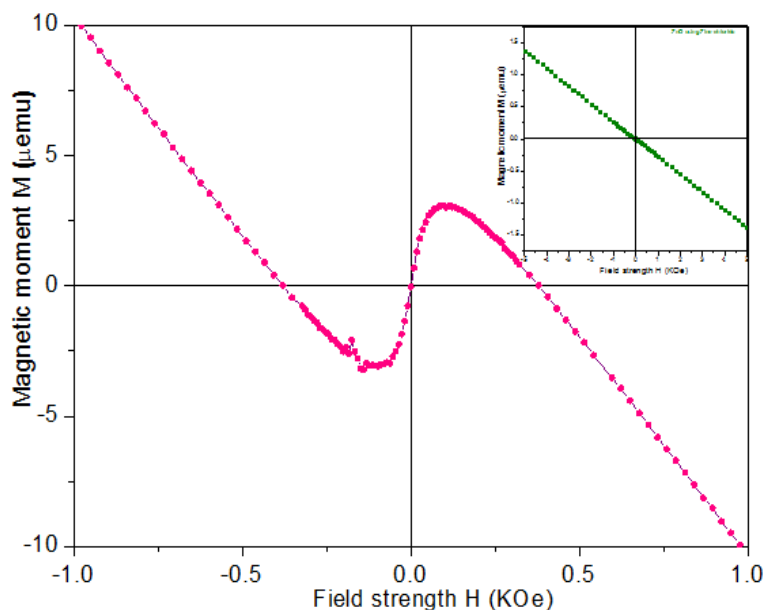
Fig. 6. M–H curves of ZnO-TiO₂ nanocomposites.

3.5. SEM and EDS Analysis

Scanning electron micrograph is shown in Fig. 7a. The SEM images of the ZnO-TiO$_2$ nanocomposites are spherical in shape. This spherical shape is due to the TiO$_2$ incorporated in ZnO matrix. From the SEM photographs, the sample had a uniform particle distribution. With the aid of image processing tools quantitative analysis of porosity and dimensions of the pores were processed [91]. The Fig.7, illustrates the intensity map of the image after multilevel thresholding with 6 levels of quantization. In Fig. 7c the portion which is dark is chosen and that portion was shown with white pixels in a solid black background. In Fig. 4.7d, the segmented porous space of ZnO sample which are labeled in different colors are shown. The Fig. 4.7e illustrates the pore size distributions.

The original and the final processed image of ZnO-TiO$_2$ nanocomposites were shown in the Fig. 7a and Fig. 7d. The distribution with less frequency ratio of ZnO-TiO$_2$ nanocomposites confirms their larger pore size as compared with ZnO prepared using ZnCl$_2$ as precursor. It has been found that the values of porosity, average and standard deviation of the pore size as 0.2664%, 2.6626 nm and 1.7091 nm. As compared with ZnO (0.2754 %), the porosity of nanocomposites (0.2664 %) is decreased due to addition of TiO$_2$ with ZnO matrix. Generally, porosity increase with increase in particle size due to the formation of chemical aggregate over the surface which is not smooth during the synthesis processes. Due to the reduced porosity, and the size of the pathways, the sediment is tightly packed towards the lower permeability. The average pore radius value of the synthesized composites was identified as mesoporous materials and is used for solar cell applications.

Fig. 8 shows the 3D surface roughness (grey scale (a) and color (b)) of the ZnO-TiO$_2$ nanocomposites which were revealed from SEM images using image processing tools. It is found that the surface roughness is less when compared with ZnO prepared with zinc chloride. This is due to the porosity ratio being low for this nanocomposite as compared with ZnO prepared with zinc chloride. So, it can be concluded that surface roughness is directly proportional to the porosity.
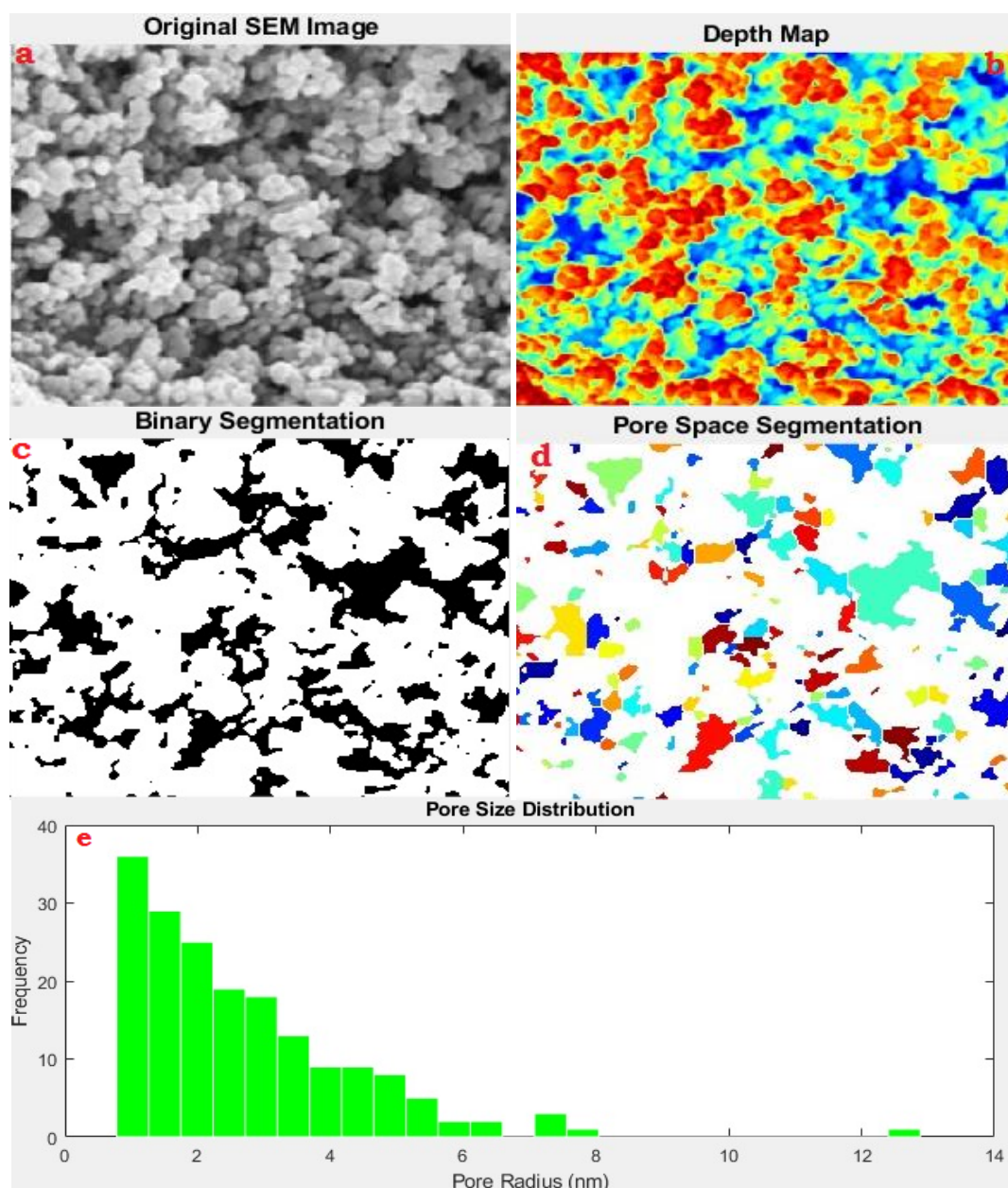
Fig. 7. SEM micrographs of ZnO-TiO₂ nanocomposites.

EDS spectra recorded during the SEM imaging technique is shown in Fig. 9. The peaks around 1.01 and 1.03keV are from the Zn La and Lb lines, and peaks observed with less counts are observed at 8.6 keV and 9.6 keV are due to Zn Ka and Zn Kb line. The peaks around 0.5keV are from the O Ka lines. The peaks around 0.452 and 0.458 keV are from the Ti La and Lb lines, and peaks observed at 4.5 keV and 4.9 keV are due to Ti Ka and Ti Kb line. It is because the incident electron will remove a Ti K-shell electron and electrons fall back from L and M shells to give discreet X-ray quanta from L to K which gives Ti Ka1 at 4.5 keV and from L to K gives Ka2 (this line is not resolvable in EDX), the transition from M to K gives a higher energy line Ti Kb at 4.9 keV. The inset picture shows the EDS of ZnO. The decrease in intensity of Zn by the increase in intensity of Ti is due to dopant which was dispersed uniformly in the ZnO matrix. It is observed that the nanoparticles contain zinc, titanium and oxygen elements predominantly.
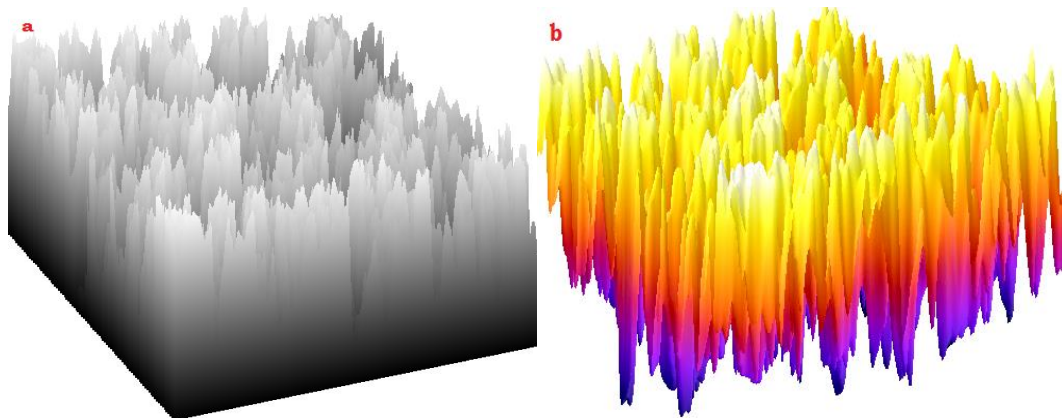
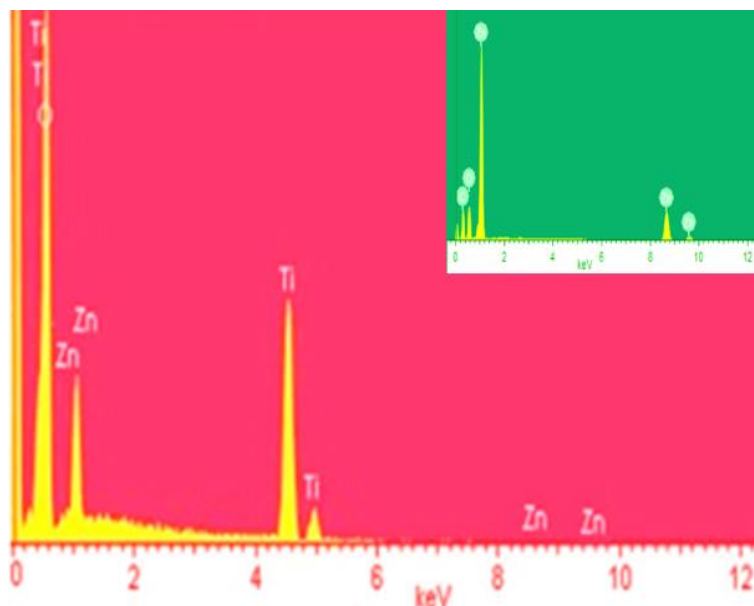*Fig. 8. Surface roughness of ZnO-TiO$_2$ nanocomposites.*

Fig. 9. EDS of ZnO-TiO$_2$ nanocomposites.

3.6. HRTEM analysis

HRTEM of the ZnO-TiO$_2$ nanocomposites is shown in Fig. 10a. The hexagonal wurtzite structure of the ZnO-TiO$_2$ nanocomposites is confirmed by the hexagonal facet and spherical structure having dimensions of 17-24nm and over the hexagonal facet and spherical structure the small particles were decorated. Image processing software tools were used to find the d spacing (Fig.10b) by employing the techniques of Inverse Fast Fourier Transform (IFFT) and Fast Fourier Transform (FFT) [87-88] and these confirm that the d space value at plane 100 reveals 0.2810 nm which was in close match with the corresponding standard values respectively. The results achieved from FFT technique were further filtered by applying Sobel filter tools to detect the defects (stacking fault and dislocation) and is plotted in Fig. 10c. The resultant micrograph was additionally processed to detect the defects in color image (Fig. 10d). The clusters of bluish green lines represent the defects (stacking fault and dislocation).
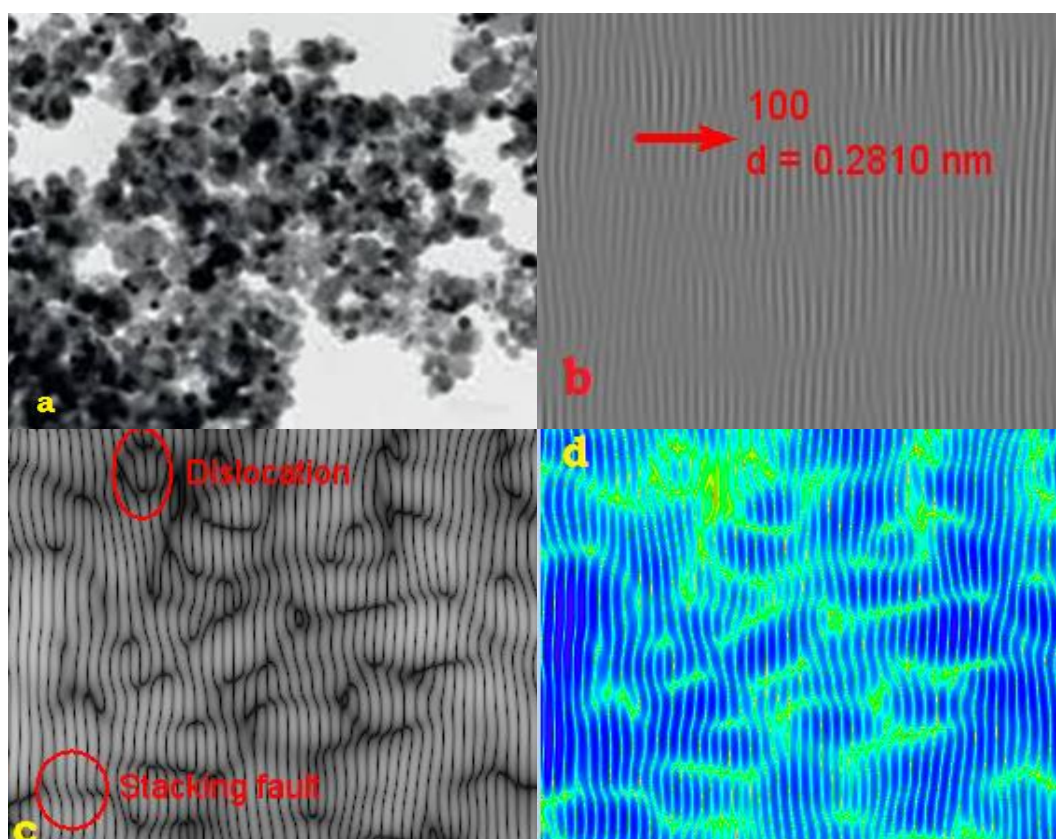
Fig. 10. HRTEM micrographs of ZnO-TiO$_2$ nanocomposites.

4 Conclusions

With the aid of sol-gel method the nanocomposites of ZnO-TiO$_2$ were synthesized by using zinc chloride, titanium tetrachloride, ethanol and benzyl alcohol and diethyl ether. The XRD patterns reveal the formation of well-crystalline single phase materials. The diffraction peaks shown at planes 100, 002, 101, 102, 110, 103, 200, 112, 201 and 202 correspond to ZnO hexagonal wurtzite phase. In addition, peaks at 101, 004, 200, 105 and 211 planes are in correspondence with TiO$_2$ anatase phase diffraction peaks. Due to the complete incorporation of TiO$_2$ in ZnO matrix, it is found that the crystallite size gets reduced as compared with ZnO nanoparticles.

From the investigations of UV-Vis spectra, the excitonic absorption peak at 380nm were observed and have sharp absorption edge which indicates the reduced particles size of ZnO. It was found that, when the conduction and valance bands expands, the band gap value was decreased in ZnO –TiO$_2$ and this cause is assigned to the variation in volume ratio of TiO$_2$ in ZnO which lead the way to modify the band gap from 3.48 eV (pure ZnO) to 3.05eV and was similar to the interaction between ZnO and TiO$_2$. In the PL spectra, the peaks giving emission at 430nm is due to the deexcitation of Ti^{3+} 3d states of ZnO-TiO$_2$ lattice from the lower vibronic level to the deep trap levels (acceptor). The peaks giving emission at 615nm is due to deexcitation of lower vibronic levels in the oxygen vacancies of TiO$_2$ lattice to the ground state. VSM study shows the existence of hysteresis curve, which confirms the ferromagnetic ordering in the specimen. From the effective SEM photographs, it has been seen that the samples have a uniform particle shape and size.

EDS result revealed that the synthesized nanocomposite contains zinc, titanium and oxygen elements predominantly. The nanocomposites exhibit in hexagonal facet and spherical like morphology with size of ~17-24 nm which confirm hexagonal wurtzite structure. The average pore

radius value of the synthesized composites was identified as mesoporous materials and are used for solar cell applications.

References

[1] R. Wahab, A. Mishra, S.I. Yun, Y.S. Kim, H.S. Shin, Applied microbiology and biotechnology, 87(5), 1917, (2010); https://doi.org/10.1007/s00253-010-2692-2

[2] C. Zhang, P.L. Yu, Y. Li, J.C. Li, Organic Electronics, 77, 105528, (2020); https://doi.org/10.1016/j.orgel.2019.105528

[3] J.M. Rzaij, A.M. Abass, Journal of Chemical Reviews, 2(2), 114, (2020); https://doi.org/10.33945/SAMI/JCR.2020.2.4

[4] I.C. Maurya, S. Singh, S. Senapati, P. Srivastava, L. Bahadur, Solar Energy, 194, 952 (2019); https://doi.org/10.1016/j.solener.2019.10.090

[5] A. Aboulouard, B. Gultekin, M. Can, M. Erol, A. Jouaiti, B. Elhadadi, C. Zafer, S. Demic, Journal of Materials Research and Technology, 9(2), 1569, (2020); https://doi.org/10.1016/j.jmrt.2019.11.083

[6] C. Sun, S. Wang, G. Ji, H. Wu, F. Huang, J. Lv,, Ferroelectrics, 529(1), 149, (2018); https://doi.org/10.1080/00150193.2018.1458532

[7] R. Qin, F. Meng, M.W. Khan, B. Yu, H. Li, Z. Fan and J. Gong, Materials Letters, 240, 84, (2019); https://doi.org/10.1016/j.matlet.2018.12.139

[8] H.K. Hakki, S. Allahyari, N. Rahemi, M. Tasbihi, Comptes Rendus Chimie, 22(5), 393, (2019); https://doi.org/10.1016/j.crci.2019.05.007

[9] L. Diamandescu, F. Vasiliu, D. Tarabasanu-Mihaila, M. Feder, A.M. Vlaicu, C.M. Teodorescu, D. Macovei, I. Enculescu, V. Parvulescu, E. Vasile, Materials Chemistry and Physics, 112(1), 2008, 146, (2008); https://doi.org/10.1016/j.matchemphys.2008.05.023

[10] T. Tong, J. Zhang, B. Tian, F. Chen, D. He, Journal of Hazardous Materials, 155(3), 572, (2008); https://doi.org/10.1016/j.jhazmat.2007.11.106

[11] K. Sabzehei, S.H. Hadavi, M.G. Bajestani, S. Sheibani, Solid State Sciences, 107, 106362, (2020); https://doi.org/10.1016/j.solidstatesciences.2020.106362

[12] B.B. Çırak, B. Caglar, T. Kılınç, S.M. Karadeniz, Y. Erdoğan, S. Kılıç, E. Kahveci, A.E. Ekinci, C. Çırak, Materials Research Bulletin, 109, 160, (2019); https://doi.org/10.1016/j.materresbull.2018.09.039

[13] X. Xu, J. Wang, J. Tian, X. Wang, J. Dai, X. Liu, Ceramics International, 37(7), 2201, (2011); https://doi.org/10.1016/j.ceramint.2011.03.067

[14] S. Haffad, K.K. Kiprono, Surface Science, 686, 10, (2019); https://doi.org/10.1016/j.susc.2019.03.006

[15] G. Marci, V. Augugliaro, M.J. López-Muñoz, C. Martín, L. Palmisano, V. Rives, M. Schiavello, R.J. Tilley, A.M. Venezia, The Journal of Physical Chemistry B, 105(5), 1026, (2001); https://doi.org/10.1021/jp003172r

[16] A. Shalaby, Y. Dimitriev, R. Iordanova, A. Bachvarova-Nedelcheva, T. Iliev, Journal of the University of Chemical Technology and Metallurgy, 46(2), 2011, 137, (2011).

[17] E.G. Goh, X. Xu, P.G. McCormick, Scripta Materialia, 78, 49, (2014); https://doi.org/10.1016/j.scriptamat.2014.01.033

[18] A.N. Mallika, A.R. Reddy, K.V. Reddy, Journal of Advanced ceramics, 4(2), 123, (2015); https://doi.org/10.1007/s40145-015-0142-4

[19] K.H. Tam, C.K. Cheung, Y.H. Leung, A.B. Djurišić, C.C. Ling, C.D. Beling, S. Fung, W.M. Kwok, W.K. Chan, D.L. Phillips, L. Ding, , The Journal of Physical Chemistry B, 110(42), 20865, (2006); https://doi.org/10.1021/jp063239w

[20] X.L. Wu, G.G. Siu, C.L. Fu, H.C. Ong, Applied Physics Letters, 78(16), 2285, (2001); https://doi.org/10.1063/1.1361288

[21] A.B. Djurišić, Y.H. Leung, Small, 2(8-9), 944, (2006);

464

https://doi.org/10.1002/smll.200600134

[22] E.P. Etape, J. Foba-Tendo, L.J. Ngolui, B.V. Namondo, F.C. Yollande, M.B.N. Nguimezong, "Structural Characterization and Magnetic Properties of Undoped and Ti-Doped ZnO Nanoparticles Prepared by Modified Oxalate Route", Journal of Nanomaterials, 2018; https://doi.org/10.1155/2018/9072325